Excitation of gigahertz magnetoelastic waves in dysprosium films: Frequency dependence*

J. T. Wang,† M. O'Donnell, and H. A. Blackstead
Department of Physics, University of Notre Dame, Notre Dame, Indiana 46556
(Received 4 August 1975)

Application of a tunable spin-phonon spectrometer to the study of microwave phonon excitations over more than an octave in frequency in polycrystalline films of dysprosium is shown to provide direct information about the coupled magnetoelastic modes. In particular, experiments demonstrate that a rf magnetic field couples to the "phononlike" branch of the magnetoelastic dispersion curves, and the attenuation of the rf field in the films leads to $q \neq 0$ momentum conservation. The observed phonon signal intensity at the rf frequency ν_0 is shown to be in excellent agreement with intensities computed from the coupled-mode dispersion relations.

I. INTRODUCTION

Results of conventional microwave magnetic resonance experiments on dysprosium[1-4] have been of interest and controversy[5-7] for a long period of time. Broad, nonresonant microwave power absorption data on single crystals of dysprosium have been difficult to understand, since, for low temperatures, the magnon energies lie above the microwave range.[8] It has been proposed[9-11] that the absorption of microwave photons by Dy is allowed by the coupling of the magnon and phonon branches of the dispersion curves. Analysis shows that "phononlike" normal modes can be excited by a low-frequency rf magnetic field. Since conventional microwave resonance experiments cannot distinguish between various processes which may contribute to the dissipation and absorption of rf power, a spin-phonon spectrometer[12] has been employed to measure the spectral composition and intensity of phonons which may result from a rf field perturbation. Tuned by the application of a static magnetic field H, this spectrometer has a frequency resolution of about 77 MHz (approximately 16 G), and a range of frequencies of approximately 10–300 GHz, the upper limit imposed by the available magnetic field strength, and the lower limit by cross relaxation.

To predict the acoustic power generated in a Dy film when irradiated by a rf magnetic field, the Hamiltonian appropriate to a thin c-plane single crystal is written in terms of magnon and phonon creation and annihilation operators, retaining only quadratic terms. The Hamiltonian was diagonalized by using the method given by White, Sparks, and Ortenburger.[13] For magnetoelastic wave propagation along the c axis, only phonons polarized parallel to the magnetization are coupled to the magnon branch, greatly simplifying the calculation. The phonon intensity is easily calculated using the rf field Hamiltonian with Fermi's "golden rule."

The intensity of phonons emitted by dysprosium films for various frequencies has been measured. It was found that the phonon intensity decreased with increasing frequency, as the theory predicted. When the polycrystalline nature of the film is considered, the calculated intensities are within a factor of 2 of those determined experimentally. Thus, the coupled-mode model appears to be the correct model to describe the magnetoelastic properties of dysprosium.

II. EXPERIMENTAL PROCEDURE AND APPARATUS

A spin-phonon spectrometer[12] has been employed to measure the frequency and intensity of phonons emitted from films of dysprosium which were evaporated onto one end of the detector element, a rectangular rod of SrF_2 doped with approximately 0.02 at.% of Tm. Approximately 50% of the Tm^{+++} was reduced to Tm^{++} by baking the crystal in an atmosphere of Sr vapor. The ground state of Tm^{++} in SrF_2 is a Kramer's doublet with an effective g factor of 3.445. At sufficiently low temperatures, the dominant relaxation mechanism is a one-phonon process. Therefore, if a static magnetic field is used to tune the doublet's splitting to the frequency of the phonons present, the phonons will be resonantly absorbed. Resonant absorption of the phonons perturbs the population levels of the ground state. The difference in population of the levels is monitored using an optical technique which exploits the strong paramagnetic circular dichroism exhibited by the Tm^{++}-SrF_2 system. The experiment is performed by measuring the circular polarization induced in an unpolarized beam of light passed through the crystal as a function of

applied field.

If an unpolarized light beam is passed through the detector, the fraction of the outgoing light which is circularly polarized is given by

$$\rho = \tanh[\alpha D \cos\theta(\Delta_l - \Delta_u)(n_l - n_u)/(\Delta_l + \Delta_u)(n_l + n_u)],$$
$$\alpha = \tfrac{1}{2}(n_l + n_u)(\Delta_l + \Delta_u), \tag{1}$$

where, in the presence of an applied dc magnetic field, n_l is the number of ions in the lower level of the doublet and n_u is the number in the upper level. Δ_l and Δ_u are the absorption cross sections, θ is the angle between the light path and the applied field direction, D is the distance the light travels in the detector, and α is the absorption coefficient. Since the circular polarization signal is sufficiently small, the hyperbolic tangent function can be replaced by its argument, such that

$$\rho = \rho_0[(n_l - n_u)/(n_l + n_u)] = \rho_0 \tanh(g\mu_B H/2KTs),$$
$$\rho_0 = \alpha D \cos\theta(\Delta_l - \Delta_u)/(\Delta_l + \Delta_u). \tag{2}$$

When a monochromatic beam of phonons at frequency ν is introduced into the system, the spin system will come into thermal equilibrium with these phonons when the static magnetic field, H_0, is varied to satisfy the conditions for ultrasonic paramagnetic resonance. Since $N(\nu_p, T_p) = (e^{h\nu_p/KT_p} - 1)^{-1}$ and $n_u/n_l = e^{-h\nu_p/KT_s}$ in thermal equilibrium, the effective phonon temperature T_p will equal the effective spin temperature T_s. The resonance conditions are

$$h\nu_p = g\mu_B(H_0 \pm \Delta H), \tag{3}$$

where u_B is the Bohr magneton and ΔH, due to Tm^{++} hyperfine splitting, is approximately 115 G. As a consequence of the hyperfine interaction, there are two resonances which are split by an equivalent field of 230 G. Also, the circularly polarized signal is due to the transitions from these two independent spin systems. The off-resonance circular polarization signal may be written

$$\rho = \rho_0 \tanh[g\mu_B(H_0 + \Delta H)/2kT_B] + \rho_0 \tanh[g\mu_B(H_0 - \Delta H)/2kT_B], \tag{4}$$

where the detector system is immersed in a helium bath at a temperature T_B. When the applied field is tuned to the lower resonance, the spin

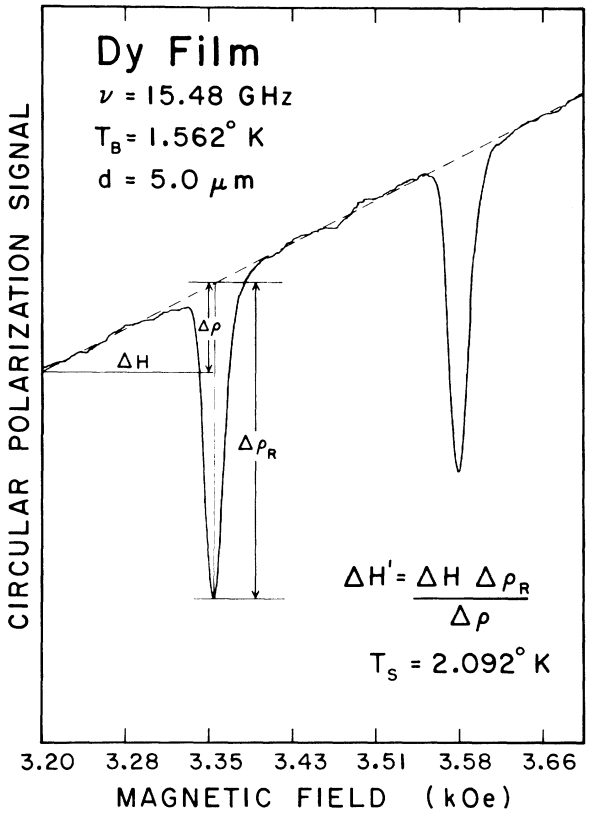

FIG. 1. Typical observation of phonons at 15.48 GHz for a dysprosium film. The two inverted peaks are due to the Tm^{++} nuclear hyperfine splitting, and the average of the two resonance fields determines the phonon frequency. The procedure to find the effective field necessary for computation of the spin temperature at resonance is illustrated.

populations of the upper resonance will not change, but those of the lower resonance will change, due to resonant phonon absorption. The circular polarization signal for the lower resonance is

$$\rho_R = \rho_0 \tanh[g\mu_B(H_0 + \Delta H)/2kT_s] + \rho_0 \tanh[g\mu_B(H_0 - \Delta H)/2kT_B]. \tag{5}$$

Figure 1 illustrates a typical signal obtained by the spin-phonon spectrometer and also illustrates a simple graphical technique to find the magnetic field $\Delta H'$ that reduces the off-resonance signal to the amplitude of the on-resonance signal. The following equation defines the relationship between $\Delta H'$ and T_s:

$$\tanh[g\mu_B(H_0 + \Delta H)/2kT_s] + \tanh[g\mu_B(H_0 - \Delta H)/2kT_B] = \tanh[g\mu_B(H_0 + \Delta H - \Delta H')/2kT_B] + \tanh[g\mu_B(H_0 - \Delta H - \Delta H')/2kT_B]. \tag{6}$$

Using a numerical method, this equation can be solved for T_s. Since $T_s = T_p$, the excess phonon density may be written

$$\epsilon = \sqrt{2}\,\rho(\nu)\Delta\nu[N(\nu, T_p) - N(\nu, T_B)]. \tag{7}$$

$\rho(\nu)$ is the phonon density of states, $\Delta\nu$ is the spectrometer linewidth, and $N(\nu, T)$ is the phonon occupation number.

Inside the rod, immersed in liquid helium, the flow of phonons can be compared to the flow of gas molecules at very low density in a porous pipe. Two scattering mechanisms affect the flow: one is momentum scattering, which removes the phonons from the frequency bandwidth of interest, and the other removes the phonons from the crystal to the helium bath. These two mechanisms contribute to a diffusion equation for the phonon density. Using the results obtained in Appendix A, the phonon density becomes

$$\epsilon(x) = \epsilon(0)e^{-x/\lambda}, \qquad \lambda = (K\tau_1)^{1/2}, \quad K = \tfrac{1}{3}v^2(\tau_1^{-1} + \tau_2^{-1})^{-1}. \tag{8}$$

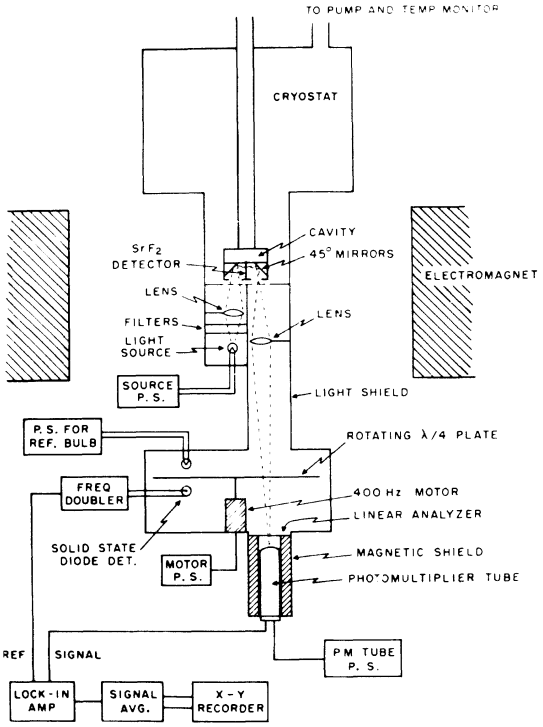

FIG. 2. Block diagram of the spin-phonon spectrometer. Unpolarized light from a small tungsten-filament bulb is passed through the SrF_2 detector, a rotating $\frac{1}{4}\lambda$ plate which is driven by a 400-Hz synchronous motor, and a linear analyzer. The light signal is detected with a photomultiplier tube, and is synchronously demodulated with a lock-in amplifier. P.S. is the abbreviation for power supply.

τ_1^{-1} is the rate of phonon losses to the bath, τ_2^{-1} is the momentum scattering rate, V is the average sound velocity, and λ is the characteristic attenuation length. Data from Ref. 12 were used for τ_1^{-1}, τ_2^{-1}, V, and λ. The quantity τ_1 was corrected for geometrical differences in the rod employed in this experiment and those of Ref. 12. Under steady-state conditions, the rate at which phonons enter the rod equals the total loss rate, such that

$$n_p = A(\tau_1^{-1} + \tau_2^{-1}) \int_0^L \epsilon(x)\,dx, \qquad n_p = A(\tau_1^{-1} + \tau_2^{-1})\epsilon(0)\lambda(1 - e^{-L/\lambda}), \tag{9}$$

where A is the cross-sectional area and L is the length of the rod. In addition to phonon losses, the acoustic impedances of the specimen and detector are not matched. The reflection and transmission coefficients[14] are given in terms of the substrate and film acoustical impedances by

$$r = (Z_f - Z_s)/(Z_f + Z_s), \qquad t = 2Z_s/(Z_f + Z_s), \quad Z = \rho V_t. \tag{10}$$

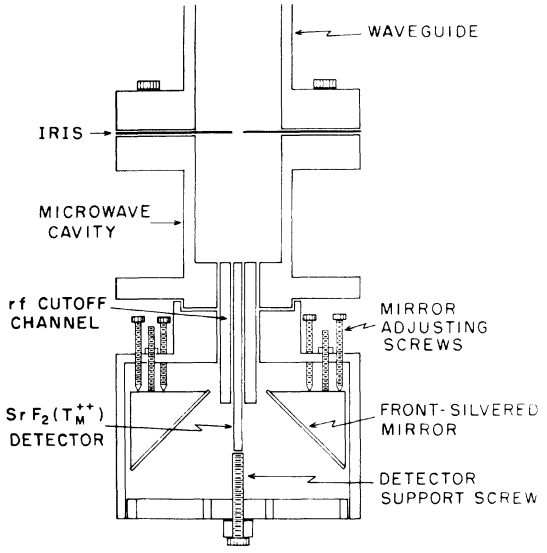

FIG. 3. Details of the cavity and optical components of the spin-phonon spectrometer. The SrF_2 detector rod is held in a rectangular channel which forms a dielectric filled wave guide with a cutoff frequency well above the operating frequency. This is essential, since the detector is very sensitive to photons. Typical rod dimensions are $0.10 \times 0.12 \times 2$ cm^3. The samples studied were evaporated to the top end of the rod and exposed to the rf magnetic field in the resonant cavity. Narrow-bandwidth (100 Å) light is reflected through the detector and into the demodulation system. Screws are provided to allow for adjustment of the front silvered mirrors.

We find $r=0.12$ and $t=0.88$, indicating that the SrF_2 is essentially transparent to phonons. The acoustical power generated at the specimen is found to be

$$P_a = h\nu n_p/t = h\nu n_p/(0.88). \tag{11}$$

By combining Eqs. (7), (9), and (11), the acoustic power emitted from the Dy film is

$$P_a = h\nu A(\tau_1^{-1}+\tau_2^{-1})\rho(\nu)\sqrt{2}\Delta\nu[N(\nu, T_p)-N(\nu, T_B)] \times e^{d/\lambda}\lambda(1-e^{-L/\lambda})/(0.88). \tag{12}$$

The block diagram of the phonon spectrometer is illustrated in Fig. 2. An interference filter with a band pass of 100 Å and a center wavelength of 5600 Å was used in conjunction with an infrared filter and a small tungsten-filament light bulb to provide the necessary light source. Since the system is also sensitive to photons, the detector must be isolated from the rf magnetic field in the microwave cavity. This is accomplished by mounting the detector in a rectangular channel which forms a dielectric-filled wave guide with a cutoff frequency much higher than the operating frequency, as can be seen in Fig. 3. This can be done to provide attenuations greater than 120 dB, and tests run with the sample films removed did not yield any signal.

III. THEORY

A. Normal modes of coupled magnetoelastic system

The analysis of this section is appropriate to easy-c-plane rare earths with the magnetization in the c plane. The simplified model Hamiltonian includes exchange, anisotropy, Zeeman, demagnetization, magnetoelastic, and elastic terms.[15,16] This Hamiltonian was obtained by rotating the standard coordinate system to place the magnetic field, H, in the basal plane parallel to the Z direction. Since we are interested in long-wavelength, low-energy excitations, complications due to the basis atom of the hcp crystal structure are ignored. Therefore, the Hamiltonian can be written

$$H = H_{ex}+H_a+H_Z+H_{me}+H_e+H_d, \tag{13}$$

where

$$H_{ex} = -\sum_{i,j} I_{ij}\vec{J}_i\cdot\vec{J}_j,$$

$$H_a = -P_2\sum_i[J_{iy}^2-\tfrac{1}{3}J(J+1)]-P_6^6\sum_i\tfrac{1}{2}(J_{i+}^6+J_{i-}^6),$$

$$H_Z = -g\mu_B\sum_i HJ_{iz},$$

$$H_{me} = -\sum_i B_{12}^{\alpha}\epsilon^{\alpha,1}\tfrac{1}{2}\sqrt{3}\,[J_{iy}^2-\tfrac{1}{3}J(J+1)]-\sum_i B_{22}^{\alpha}\epsilon^{\alpha,2}\tfrac{1}{2}\sqrt{3}\,[J_{iy}^2-\tfrac{1}{3}J+1)] -\sum_i B^{\gamma}[\tfrac{1}{2}\epsilon_1^{\gamma}(J_{ix}^2-J_{iz}^2)+\tfrac{1}{2}\epsilon_2^{\gamma}(J_{ix}J_{iz}+J_{iz}J_{ix})]-\sum_i B^{\epsilon}[\tfrac{1}{2}\epsilon_1^{\epsilon}(J_{iz}J_{iy}+J_{iy}J_{iz})+\tfrac{1}{2}\epsilon_2^{\epsilon}(J_{ix}J_{iy}+J_{iy}J_{ix})], \tag{14}$$

$$H_d = \tfrac{1}{2}g\mu_B\sum_i D_z M_z J_{iz}+D_x M_x J_{ix}+D_y M_y J_{iy},$$

$$H_e = \int_V\{\tfrac{1}{2}C_{12}^{\alpha}(\epsilon^{\alpha,1})^2+C_{12}^{\alpha}\epsilon^{\alpha,1}\epsilon^{\alpha,2}+\tfrac{1}{2}C_{22}^{\alpha}(\epsilon^{\alpha,2})^2+\tfrac{1}{2}C^{\gamma}[(\epsilon_1^{\gamma})^2+(\epsilon_2^{\gamma})^2]+\tfrac{1}{2}C^{\epsilon}[(\epsilon_1^{\epsilon})^2+(\epsilon_2^{\epsilon})^2]\}\,dV + \tfrac{1}{2}\rho\int_V\sum_{\mu=1}^{3}\left(\frac{du_\mu}{dt}\right)^2 dV.$$

The symmetry strains and elastic constants used here are the same as those defined in Ref. 16. We will write the strains in a small oscillations approach, such that

$$\epsilon_{\mu\nu} = \bar{\epsilon}_{\mu\nu}(\vec{\alpha})+\epsilon_{\mu\nu}(\vec{q},\omega), \tag{15}$$

where[17] $\epsilon(\vec{q},\omega)$ is the time and wave-vector-dependent strain and $\bar{\epsilon}_{\mu\nu}(\vec{\alpha})$ is the equilibrium strain as a function of the direction cosines of the magnetization. Using the standard Holstein-Primakoff transformations[18] for the angular momentum operators and the phonon expansion[17] for the time-dependent strain, the Hamiltonian becomes

$$H = H_0 + \sum_{\vec{q}} [A_{\vec{q}}\, \alpha_{\vec{q}}^{\dagger}\, \alpha_{\vec{q}} + B_{\vec{q}}(\alpha_{\vec{q}}\, \alpha_{-\vec{q}} + \alpha_{\vec{q}}^{\dagger}\, \alpha_{-\vec{q}}^{\dagger})]$$

$$+ \sum_{\vec{q},p} [\Delta_{\vec{q},p}\, \alpha_q (\beta_{-\vec{q},p} + \beta_{\vec{q},p}^{\dagger}) + \Delta_{\vec{q},p}^{*}\, \alpha_{\vec{q}}^{\dagger} (\beta_{-\vec{q},p}^{\dagger} + \beta_{\vec{q},p})] + \sum_{\vec{q},p} \hbar\omega_{\vec{q},p} \beta_{\vec{q},p}^{\dagger} \beta_{\vec{q},p}, \tag{16}$$

where

$$A_{\vec{q}} = 2J[I(0) - I(\vec{q})] + 21P_6^6 J^5 - P_2 J + \tfrac{3}{2}\bar{\epsilon}_1^{\gamma}(\vec{\alpha}) B^{\gamma} J$$
$$+ g\mu_B H - D_z M + \tfrac{1}{2} M (D_x + D_y) - \tfrac{1}{2}\sqrt{3} J[B_{12}^{\alpha} \bar{\epsilon}^{\alpha,1}(\vec{\alpha}) + B_{22}^{\alpha} \bar{\epsilon}^{\alpha,2}(\vec{\alpha})],$$

$$B_{\vec{q}} = \tfrac{15}{2} P_6^6 J^5 + \tfrac{1}{2} P_2 J + J\bar{\epsilon}_1^{\gamma}(\vec{\alpha}) \tfrac{1}{4} B^{\gamma} + \tfrac{1}{4} g\mu_B M (D_x - D_y) + \tfrac{1}{4}\sqrt{3} J[B_{12}^{\alpha} \bar{\epsilon}^{\alpha,1}(\vec{\alpha}) + B_{22}^{\alpha} \bar{\epsilon}^{\alpha,2}(\vec{\alpha})], \tag{17}$$

$$\Delta_{\vec{q},p} = -\tfrac{1}{2} J^{3/2} \{(\hbar\omega_{\vec{q},p}/m V_{\vec{q},p}^2)^{1/2} [B^{\epsilon}(e_{\vec{q},p}^{y} \sigma_z + e_{\vec{q},p}^{z} \sigma_z) + i B^{\gamma}(e_{\vec{q},p}^{x} \sigma_z + e_{\vec{q},p}^{z} \sigma_y)]\}.$$

The B's are the magnetoelastic coupling constants, $\hbar\omega_{\vec{q},p}$ is the unperturbed phonon energy, M is the magnitude of the magnetization, m is the mass of the unit cell, $V_{\vec{q},p}$ is the velocity of the elastic wave, σ_ν is the direction cosine of the wave vector with respect to the ν axis, and J is the expectation value of J_z.

Using the procedure given by White, Sparks, and Ortenburger,[13] diagonalization of the Hamiltonian is straightforward, and can be written

$$H = \sum_{\vec{q},p} (\Omega_{\vec{q},p}^{+} \gamma_{\vec{q},p}^{\dagger} \gamma_{\vec{q},p} + \Omega_{\vec{q},p}^{-} \delta_{\vec{q},p}^{\dagger} \delta_{\vec{q},p}). \tag{18}$$

The coupled-mode energies are given by

$$\Omega_{\vec{q},p}^{\pm} = \sqrt{\tfrac{1}{2}} ((A_{\vec{q}}^2 - 4B_{\vec{q}}^2 + \hbar^2\omega_{\vec{q},p}^2) \pm (A_{\vec{q}}^2 - 4B_{\vec{q}}^2 - \hbar^2\omega_{\vec{q},p}^2)^2$$
$$+ 16\hbar\omega_{\vec{q},p} \{A_{\vec{q}} |\Delta_{\vec{q},p}|^2 + B_{\vec{q}}[(\Delta_{\vec{q},p}^{*})^2$$
$$+ (\Delta_{\vec{q},p})^2]\}^{1/2})^{1/2}, \tag{19}$$

and the new normal-mode operators (γ's and δ's) are related to the α's and B's by the transformation matrix S_{ij} which diagonalizes the Hamiltonian. The transformation matrix is defined by $X = SX'$, where

$$X = \begin{bmatrix} \alpha_{\vec{q}} \\ \alpha_{-\vec{q}}^{\dagger} \\ B_{\vec{q},p} \\ B_{-\vec{q},p}^{\dagger} \end{bmatrix}, \quad X' = \begin{bmatrix} \gamma_{\vec{q},p} \\ \gamma_{-\vec{q},p}^{\dagger} \\ \delta_{\vec{q},p} \\ \delta_{-\vec{q},p}^{\dagger} \end{bmatrix}. \tag{20}$$

For waves propagating along the c axis, only one phonon mode is coupled to the magnons. In Fig. 4, $\Omega_{\vec{q},p}^{-}$ is plotted for two different polarizations. Since a wave polarized perpendicular to the magnetization decouples, Fig. 4 indicates the strength of the magnetoelastic interaction for long wavelengths. In Fig. 5, the "phononlike" mode is plotted versus applied field. As is illustrated by these figures, the normal modes of the coupled system can no longer be easily distinguished as being magnetic (magnon) or elastic (phonon) modes, since the new modes are complicated mixtures of both types of excitations. For $\vec{q} = 0$, the case of uniform precession, the system decouples, leaving only the so-called

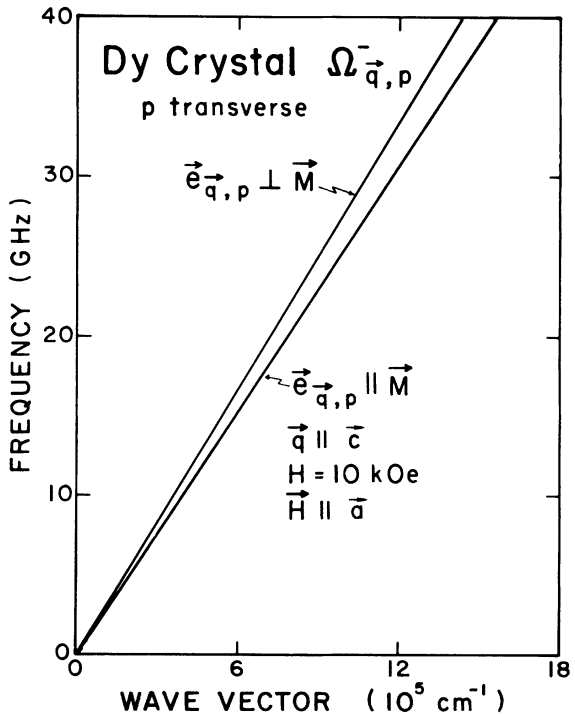

FIG. 4. $\Omega_{\vec{q},T}^{-}$ for transverse waves propagating along the c axis, polarized parallel and perpendicular to the magnetization. For perpendicular polarization, the magnetoelastic coupling vanishes, in this approximation, leaving a "pure" phonon mode. The magnetoelastic coupling has removed the degeneracy of waves propagating parallel to the c axis.

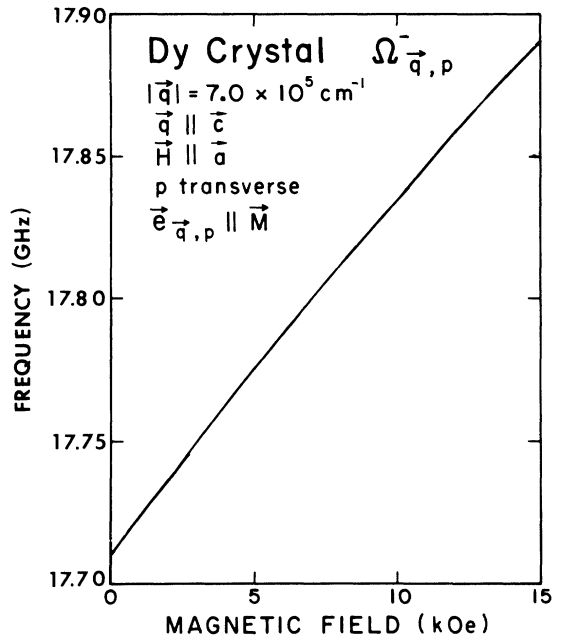

FIG. 5. Field dependence of $\bar{\Omega}_{\vec{q},T}$ ($\vec{e}_{q,T} \| \vec{M}$). The phononlike branch does not exhibit strong field dependence, thereby permitting use of the spin-phonon spectrometer, for which the field and frequency are not independent variables.

frozen-lattice[7] contribution in the magnon energy expression.

B. rf magnetic field perturbation

For a rf magnetic field applied along the x axis, the interaction Hamiltonian can be written

$$H_{\rm int} = -g\mu_B \sum_i H_{\rm rf} J_{ix}. \tag{21}$$

Since a rf magnetic field is attentuated as it penetrates into a metal, it may be written

$$H_{\rm rf} = H^0_{\rm rf}\, e^{-i\omega t} e^{-y/\Delta} \cos(y/\Delta), \tag{22}$$

where Δ is the usual microwave skin depth.[19] Using the standard Holstein-Primakoff[18] transformation for the angular momentum operators, the interaction Hamiltonian becomes

$$H_{\rm int} = -g\mu_B H^0_{\rm rf} e^{-i\omega t} \sum_{i,\vec{q}} e^{-y/\Delta} \cos(y/\Delta) \times e^{i(\vec{q}\cdot\vec{R}_i)} (J/2N)^{1/2} (\alpha_{\vec{q}} + \alpha^\dagger_{-\vec{q}}). \tag{23}$$

The summation over y is replaced by an integration from 0 to d, the sample thickness, yielding

$$H_{\rm int} = C_1 e^{-i\omega t} \sum_q f(q)(\alpha_q + \alpha^\dagger_{-q}),$$
$$C_1 = -g\mu_B H^0_{\rm rf} (2JN)^{1/2}, \tag{24}$$

$$f(q) = \frac{e^{-d/\Delta} e^{i(q+1/\Delta)d} - 1}{2d[(1/\Delta)^2 + (1/\Delta + q)^2]} \left[i\left(\frac{1+i}{\Delta} + q\right)\right] + \frac{e^{-d/\Delta} e^{-i(1/\Delta - q)d} - 1}{2d[(1/\Delta)^2 + (1/\Delta - q)^2]} \left[i\left(\frac{i-1}{\Delta} + q\right)\right],$$

where $q = |\vec{q}| = q_y$ and $N_y = d/c$ have been used. In order to proceed further, the magnon operators α_q and $\alpha^\dagger_{-q}$ must be expressed in terms of the normal modes of the system by making use of the transformation matrix S_{ij}. Having done this, the perturbation Hamiltonian for waves propagating along the c axis becomes

$$H_{\rm int} = C_1 e^{-i\omega t} \sum_q f(q)[S_{11}(q) + S_{21}(q)]\gamma_{q,T} + [S_{12}(q) + S_{22}(q)]\gamma^\dagger_{-q,T} + [S_{13}(q) + S_{23}(q)]\delta_{q,T} + [S_{14}(q) + S_{24}(q)]\delta^\dagger_{-q,T}, \tag{25}$$

where the subscript T refers to a transverse polarization. Since the $\Omega^+_{q,T}$ energies are much higher than the microwave frequencies used in these experiments, we are only interested in the $\Omega^-_{q,T}$ branch of the dispersion curve. Now, since $S_{ij}(q) = S_{ij}(-q)$, and since

$$S_{14}(q) + S_{24}(q) = S_{13}(q) + S_{23}(q), \tag{26}$$

where

$$S_{14}(q) + S_{24}(q) = [16\hbar^2 \omega^2_{q,T}(A^2_q - 4B^2_q)^{1/2} \times |\Delta_{q,T}|^2]^{1/2}/N,$$
$$N = [16\hbar^2 \omega^2_{q,T} \Omega^-_{q,T}(A^2_q - 4B^2_q)^{1/2} |\Delta_{q,T}|^2 + 4\Omega^-_{q,T} \hbar\omega_{q,T}(\Omega^{-2}_{q,T} + 4B^2_q - A^2_q)^2]^{1/2} \tag{27}$$

then, the perburbation Hamiltonian becomes

$$H_{\rm int} = C_1 e^{-i\omega t} \sum_q f(q)[S_{14}(q) + S_{24}(q)] \times (\delta^\dagger_{q,T} + \delta_{q,T}). \tag{28}$$

Using Fermi's golden rule for transition rates, the total microwave power absorbed can be computed:

$$P_{\rm abs} = 2\pi\omega_0 (|\langle n^\delta_{q,T} + 1| H_{\rm int} | n^\delta_{q,T}\rangle|^2 - |\langle n^\delta_{q,T}| H_{\rm int} | n^\delta_{q,T} + 1\rangle|^2) \delta(\Omega^-_{q,T} - \hbar\omega_0). \tag{29}$$

Replacing the sum over q by an integral and approximating $\Omega^-_{q,T}$ by $\hbar\omega_{q,T}$, then the total power absorbed becomes

$$P_{\rm abs} = 2\omega_0 d C_1^2 |f(\omega_0/V_{q,T})|^2 |S_{14}(\omega_0/V_{q,T}) + S_{24}(\omega_0/V_{q,T})|^2/\hbar V_{q,T}, \tag{30}$$

where $\omega_0/2\pi$ is the microwave driving frequency.

In order to compute the acoustic power generated, we must determine the relative intensity of the elastic part of the δ excitation. Since

$$\begin{aligned}\beta_{q,T} &= S_{31}(q)\gamma_{q,T} + S_{32}(q)\gamma^{\dagger}_{-q,T} + S_{33}(q)\delta_{q,T} \\ &\quad + S_{34}(q)\delta^{\dagger}_{-q,T}, \\ \beta^{\dagger}_{q,T} &= S_{41}(q)\gamma_{q,T} + S_{42}(q)\gamma^{\dagger}_{-q,T} + S_{43}(q)\delta_{q,T} \\ &\quad + S_{44}(q)\delta^{\dagger}_{-q,T},\end{aligned} \tag{31}$$

then

$$\langle n^{\delta}_{q,T} | \beta^{\dagger}_{q,T}\beta_{q,T} | n^{\delta}_{q,T}\rangle = S_{33}(q)S_{44}(q)n^{\delta}_{q,T}, \tag{32}$$

and so the acoustic power becomes

$$\begin{aligned}P_{\text{acous.}} &= [\,2\omega_0 d C_1^2 |f(\omega_0/V_{q,T})|^2 |\,S_{14}(\omega_0/V_{q,T}) \\ &\quad + S_{24}(\omega_0/V_{q,T})|^2 \\ &\quad \times S_{33}(\omega_0/V_{q,T})S_{44}(\omega_0/V_{q,T})]\,/\hbar V_{q,T},\end{aligned} \tag{33}$$

where $S_{33} \approx S_{44} \approx 0.98$ and therefore almost all the power absorbed by the δ mode appears as acoustic power. Calculations using the above equations can be directly compared to experimentally determined phonon intensities for polycrystalline films. See Appendix B.

IV. RESULTS AND CONCLUSIONS

A large number of films of varying thicknesses were evaporated on several different detectors. Films with a thickness of several μm were found to yield optimal signals.[16] The highest quality detector available was employed to measure the phonon emission at the rf magnetic field frequency from a 5.0-μm dysprosium film as a function of power input to the cavity, frequency of the rf field, and angle between the rf and dc fields. Studies of power dependence show that the phonon signal is proportional to the power input to the cavity, as is expected from above. As can be ascertained from Fig. 6, essentially no angular dependence has been observed for dysprosium films when both the rf and dc fields are applied in the plane of the film. Since the spectrometer response is isotropic to magnetic field direction,[12] this result is seen to be a consequence of the uniaxial anisotropy present in the randomly oriented crystallites which make up the film. The effective anisotropy field is much larger than the magnetic fields applied in these low temperature experiments.[20] Therefore, since the effective basal plane anisotropy field is small, we anticipate that only those crystallites oriented with their basal planes parallel to the rf magnetic field will make substantial contributions to the absorption of rf power.

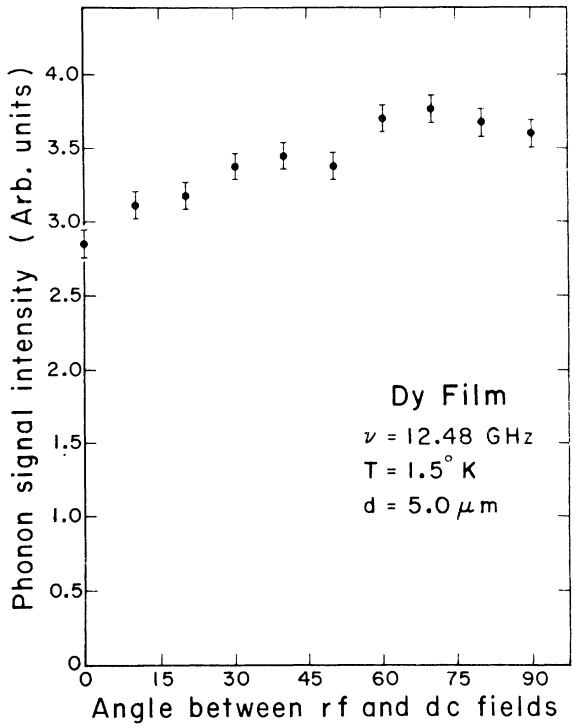

FIG. 6. Phonon signal intensity from a 5-μm dysprosium film at 12.48 GHz as a function of the angle between the rf and dc fields. It is noted that the signal does not depend strongly on the angle, apparently a result of the polycrystalline character of the film.

Strong dependence on the excitation frequency has also been observed, with stronger signals occurring at lower frequencies. Figure 7 shows the striking similarity between phonon intensities calculated using the coupled-mode analysis and signals detected using the spin-phonon spectrometer. In Fig. 7 the solid line corresponds to phonon emission from a single crystal film. Since the films employed in this study were polycrystalline, a procedure had to be developed to account for the polycrystalline nature of the specimen.

For a polycrystalline film, the Hamiltonian should be diagonalized for an arbitrary orientation of the crystallite relative to the rf and dc field direction. Then, an average over all crystallites of the power emitted from each crystallite must be performed. Because of dysprosium's large uniaxial anisotropy, the magnetization must lie in the basal plane of each crystallite, and so only transverse phonons can be excited. The Hamiltonian, in this case, is a six by six and can be numerically diagonalized. Although this can be done, no new physical information would be gained, since propagation in directions other than the c direction is governed by coupling con-

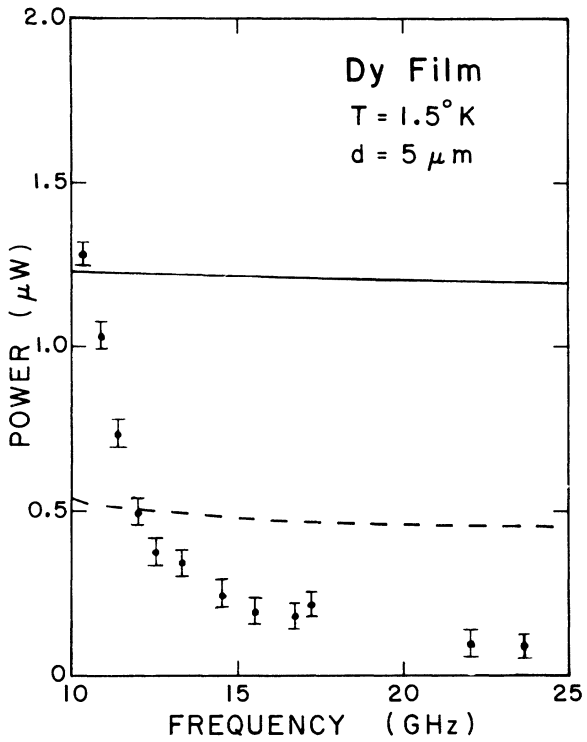

FIG. 7. Theoretical and experimental phonon signal intensity for a 5-μm film as a function of frequency. The solid line is the calculated intensity for an unrealistic single crystal film and the dashed line is an estimate of the theoretical acoustic power from a polycrystalline film. The data and experiments are in excellent agreement, providing a quantitative verification of the coupled-mode analysis.

stants of approximately the same size as those governing c-axis propagation. The power emitted from a polycrystalline film, therefore, is adequately represented by an average over all crystallites using only the Hamiltonain for c-axis propagation. This average would yield the polycrystalline magnetization. Thus, a rough estimate of the effect of the film being polycrystalline can be made by renormalizing the magnetization, and all magnetization-dependent terms such as the equilibrium strains, to the magnetization measurements of polycrystalline dysprosium made by Elliott, Legvold, and Spedding.[21] The phonon emission calculated using this magnetization and the results of Appendix B has been plotted in Fig. 7 as a dashed line. At all frequencies the agreement in absolute signal size between the experimentally determined phonon signal and that obtained from a coupled mode analysis is good. Although the experimentally determined phonon power decreases with increasing frequency more rapidly than predicted, the data and calculated signal intensities still agree within a factor of 2 for all frequencies.

The phonon signals obtained in this study were generated through the direct coupling of the rf magnetic field to the "phononlike" δ mode of the coupled-mode Hamiltonian. The frequencies used in this experiment were far from the crossover frequency (350 GHz). If the driving frequency (which, at these frequencies, must come from an infrared source) were tuned to crossover, then dysprosium could act as a high-frequency, monoergic phonon source, except for the fact that the absolute signal size will be severly damped by $f(q)$ at the q values necessary for crossover. If the maximum of $f(q)$ could be shifted near the q which corresponds to crossover, then dysprosium could be used as a high-frequency, high-power-level phonon source. The best solution may be to construct thin films which have thickness related standing-wave modes of magnetoelastic character.[22]

APPENDIX A: DERIVATION OF DIFFUSION EQUATION FOR PHONON SPECTROMETER

From the conservation of phonon current, we can state that

$$\frac{d\rho}{dt} + \vec{\nabla}\cdot(\rho\vec{V}) - L = 0, \tag{A1}$$

where L represents the losses and ρ is the number of phonons of frequency ν per unit volume, moving in the direction $\hat{k}$. Let $\rho = f(\vec{x}, \vec{k}) = \rho(\vec{x})\phi(\vec{k})$ and phonons can be lost to the bath or by momentum scattering. Therefore, the diffusion equation becomes, following Ref. 12,

$$0 = \frac{df(\vec{x},\vec{k})}{dt} + \vec{\nabla}\cdot[\rho(\vec{x})\phi(\vec{k})\vec{V}] - \tau_1^{-1}(\rho\phi - \rho_e) - \tau_2^{-1}(\rho\phi - \rho), \tag{A2}$$

where τ_1^{-1} is the loss rate to the bath, ρ_e is the number of phonons per unit volume in the bath, and τ_2^{-1} is the rate phonons are scattered out of the momentum band of interest. Now, for an isotropic crystal $\vec{\nabla}\cdot\vec{V} = 0$, and for phonons propagating in the k direction, then $\vec{V} = V\hat{k}$ and

$$\vec{\nabla}\cdot(\rho\phi\vec{V}) = V\hat{k}\,\nabla(\rho\phi). \tag{A3}$$

The diffusion equation becomes

$$-\frac{df}{dt} = V\hat{k}\,\nabla(\rho\phi) + \tau_1^{-1}(\rho_e - \rho\phi) + \tau_2^{-1}(1-\phi)\rho. \tag{A4}$$

Now the average density $\rho(x)$ of phonons at the point x is given by an average over all propagation directions:

$$\rho(\vec{x}) = \frac{1}{4\pi} \int f(\vec{x}, \vec{k})\, d\Omega_{\vec{k}}. \tag{A5}$$

And the phonon current becomes

$$\vec{j}(x) = \frac{V}{4\pi} \int \hat{k} f(\vec{x}, \vec{k})\, d\Omega_{\vec{k}}$$

$$= \frac{V\rho(\vec{x})}{4\pi} \int \hat{k}\phi(\vec{k})\, d\Omega_{\vec{k}}, \tag{A6}$$

where

$$\frac{1}{4\pi} \int \phi(\vec{k})\, d\Omega_{\vec{k}} = 1. \tag{A7}$$

Now, for steady-state conditions $df/dt = 0$, therefore $\phi(\vec{k})$ becomes

$$\phi(\vec{k}) = [\rho(\vec{x})(\tau_1^{-1} + \tau_2^{-1})]^{-1}[\, V\hat{k}\cdot\vec{\nabla}(\rho\phi) + \tau_1^{-1}\rho_e + \tau_2^{-1}\rho\,]. \tag{A8}$$

And, therefore, the phonon current becomes

$$\vec{j}(\vec{x}) = \frac{V}{4\pi(\tau_1^{-1} + \tau_1^{-1})} \int [\, V\hat{k}\cdot\vec{\nabla}(\rho\phi) + \tau_1^{-1}\rho_e + \tau_2^{-1}\rho\,]\, d\Omega_{\vec{k}}. \tag{A9}$$

The last two terms in this expression vanish since they are proportional to $\hat{k}$, where

$$\int \hat{k}\, d\Omega_{\vec{k}} = 0. \tag{A10}$$

Therefore,

$$\vec{j}(\vec{x}) = \frac{V^2}{\tau_1^{-1} + \tau_2^{-1}} \int V\hat{k}\cdot\vec{\nabla}(\rho\phi)\hat{k}\, d\Omega_{\vec{k}}. \tag{A11}$$

For the α component of the current we obtain

$$j_\alpha(\vec{x}) = \frac{V^2}{\tau_1^{-1} + \tau_2^{-1}} \frac{d\rho}{dx_\alpha} \int \frac{k_\alpha^2 \phi(k_\alpha)\, d\Omega_k}{4\pi} = k_\alpha \frac{d\rho}{dx_\alpha}. \tag{A12}$$

For an isotropic distribution $\phi(k) = 1$, and therefore

$$j_\alpha(\vec{x}) = \tfrac{1}{3}V^2(\tau_1^{-1} + \tau_2^{-1})^{-1}\frac{d\rho}{dx_\alpha},$$
$$\vec{\nabla}\cdot\vec{j}(\vec{x}) = \tfrac{1}{3}V^2(\tau_1^{-1} + \tau_2^{-1})^{-1}\nabla^2\rho(\vec{x}). \tag{A13}$$

Now, since $\nabla^2\rho_e = 0$, then let $\epsilon = \rho - \rho_e$, thus $\nabla^2\rho = \nabla^2\epsilon$, and the divergence of the current becomes

$$\vec{\nabla}\cdot\vec{j} = \tfrac{1}{3}V^2(\tau_1^{-1} + \tau_2^{-1})^{-1}\nabla^2\epsilon. \tag{A14}$$

Now

$$\vec{\nabla}\cdot\vec{j} = \frac{1}{4\pi} \int V\hat{k}\cdot\vec{\nabla}(\rho\phi)\, d\Omega_{\vec{k}}, \tag{A15}$$

but, under steady-state conditions

$$V\hat{k}\cdot\vec{\nabla}(\rho\phi) = \tau_1^{-1}(\rho\phi - \rho_e) + \tau_2^{-1}(\phi - 1)\rho. \tag{A16}$$

Therefore,

$$\vec{\nabla}\cdot\vec{j} = \frac{1}{4\pi} \int [\tau_1^{-1}(\rho\phi - \rho_e) + \tau_2^{-1}(\phi - 1)\rho]\, d\Omega_{\vec{k}}, \tag{A17}$$

but

$$\frac{1}{4\pi} \int \phi(\vec{k})\, d\Omega_{\vec{k}} = 1,$$

and so

$$\vec{\nabla}\cdot\vec{j} = (\rho - \rho_e)\tau_1^{-1},$$
$$\vec{\nabla}\cdot\vec{j} = \epsilon\tau_1^{-1}. \tag{A18}$$

Therefore,

$$\tfrac{1}{3}V^2(\tau_1^{-1} + \tau_2^{-1})\nabla^2\epsilon = \epsilon\tau_1^{-1}. \tag{A19}$$

And so $\epsilon(x)$ is exponentially damped, such that

$$\epsilon(x) = \epsilon_0 e^{-x/\lambda}, \tag{A20}$$

where $\lambda = (\kappa\tau_1)^{1/2}$, where

$$\kappa = \tfrac{1}{3}V^2(\tau_1^{-1} + \tau_1^{-1})^{-1}. \tag{A21}$$

APPENDIX B

Following the procedure of Bozorth and Wakiyama,[23] the magnetostriction of a film of randomly oriented hexagonal crystallites can be easily computed. For a hexagonal single crystal the magnetostriction is

$$\lambda = (\tfrac{1}{3}\bar{\epsilon}^{\alpha,1} - \tfrac{1}{3}\sqrt{3}\,\bar{\epsilon}^{\alpha,2} + \bar{\epsilon}_1^{\gamma})\beta_z^2 + (\tfrac{1}{3}\bar{\epsilon}^{\alpha,1} - \tfrac{1}{3}\sqrt{3}\,\bar{\epsilon}^{\alpha,2} - \bar{\epsilon}_1^{\gamma})\beta_x^2 + (\tfrac{1}{3}\bar{\epsilon}^{\alpha,1} + \tfrac{1}{3}\sqrt{3}\,\bar{\epsilon}^{\alpha,2})\beta_y^2 + 2\bar{\epsilon}_2^{\gamma}\beta_z\beta_x + 2\bar{\epsilon}_1^{\epsilon}\beta_x\beta_y + 2\bar{\epsilon}_2^{\epsilon}\beta_z\beta_y, \tag{B1}$$

where

$$\bar{\epsilon}^{\alpha,1} = \lambda_{11}^{\alpha} + \lambda_{12}^{\alpha}\tfrac{1}{2}\sqrt{3}\,(\alpha_y^2 - \tfrac{1}{3}),$$
$$\bar{\epsilon}^{\alpha,2} = \lambda_{21}^{\alpha} + \lambda_{22}^{\alpha}\tfrac{1}{2}\sqrt{3}\,(\alpha_y^2 - \tfrac{1}{3}),$$
$$\bar{\epsilon}_1^{\gamma} = \tfrac{1}{2}\lambda^{\gamma}(\alpha_z^2 - \alpha_x^2), \quad \bar{\epsilon}_2^{\gamma} = \lambda^{\gamma}\alpha_x\alpha_z,$$
$$\bar{\epsilon}_1^{\epsilon} = \lambda^{\epsilon}\alpha_x\alpha_y, \quad \bar{\epsilon}_2^{\epsilon} = \lambda^{\epsilon}\alpha_z\alpha_y, \tag{B2}$$

and where the α's and β's are, respectively, the direction cosines of the saturation magnetization and the gauge. Let ϕ be the angle in the x-z plane, θ the angle from the c axis, and θ_0 the angle between the easy direction and the c axis. Then λ can be calculated in any direction by evalu-

ating $\lambda = \lambda(\theta, \phi) - \lambda(\theta_0, 0)$. Using the above expression for the magnetostriction, and writing the direction cosines in terms of θ and ϕ, λ becomes

$$\lambda = \{\tfrac{1}{3}\lambda_{11}^{\alpha} + (\cos^2\theta - \cos^2\theta_0)[(1/2\sqrt{3})\lambda_{12}^{\alpha} - \tfrac{1}{2}\lambda_{22}^{\alpha}] - \tfrac{1}{3}\sqrt{3}\,\lambda_{21}^{\alpha}\}\sin^2\theta$$
$$+ \tfrac{1}{2}\lambda^{\gamma}\{[\sin^2\theta(\cos^2\phi - \sin^2\phi) - \sin^2\theta_0][\sin^2\theta(\cos^2\phi - \sin^2\phi)]\}$$
$$+ 2\gamma\sin^4\theta\sin^2\phi\cos^2\phi + 2\lambda^{\epsilon}\sin^2\theta\cos^2\theta\sin^2\phi + 2\lambda^{\epsilon}(\sin^2\theta\cos^2\theta\cos^2\phi - \sin\theta\cos\theta\sin\theta_0\cos\theta_0\cos\phi). \quad \text{(B3)}$$

In order to account for the polycrystalline nature of the film, the magnetostriction must be averaged over all possible gauge directions. Thus, ϕ must be averaged over π ($\langle\langle \sin\phi\rangle = \langle\cos\phi\rangle = 0$, $\langle\sin^2\phi\rangle = \frac{1}{2}$) and θ must be averaged over a sphere ($\langle\langle \sin^2\theta\rangle = \frac{2}{3}, \ldots$) such that

$$\bar{\lambda} = \tfrac{2}{15}\{\tfrac{5}{3}\lambda_{11}^{\alpha} + (\lambda_{12}^{\alpha}/\sqrt{3})(1 - \tfrac{5}{2}\cos^2\theta_0)$$
$$- (5/\sqrt{3})\lambda_{21}^{\alpha} + \lambda_{22}^{\alpha}(\tfrac{5}{2}\cos^2\theta_0 - 1)\} + \tfrac{4}{15}(\lambda^{\gamma} + \lambda^{\epsilon}). \quad \text{(B4)}$$

In a hexagonal crystal with large uniaxial anisotropy and an easy plane, $\theta_0 = \frac{1}{2}\pi$ in each crystallite. As a result $\cos\theta_0 = 0$ and $\bar{\lambda}$ becomes

$$\bar{\lambda} = \tfrac{2}{15}(\tfrac{5}{3}\lambda_{11}^{\alpha} + \tfrac{1}{3}\sqrt{3}\,\lambda_{12}^{\alpha} - \tfrac{5}{3}\lambda_{21}^{\alpha} - \lambda_{22}^{\alpha}) + \tfrac{4}{15}(\lambda^{\alpha} + \lambda^{\epsilon}). \quad \text{(B5)}$$

Previously, the strains have been written in a small oscillations approximation:

$$\epsilon_{\mu\nu} = \bar{\epsilon}_{\mu\nu}(\vec{\alpha}) + \epsilon_{\mu\nu}(\vec{q}, \omega). \quad \text{(B6)}$$

Since the strains are changed by the polycrystalline average, it is appropriate to consider the averaging for the dynamic strains. In particular, $\bar{\epsilon}_2^{\epsilon}$, the driven mode, is proportional to λ^{ϵ} which is reduced in amplitude from the single-crystal value by a factor of $\frac{4}{15}$. As a result, the phonon power resulting from the time dependence of ϵ_2^{ϵ} must be multiplied by $(\frac{4}{15})^2$. This factor has been included in the polycrystalline power calculation given in Fig. 7. Of course, phonons are also excited in the basal plane of properly oriented crystallites in the polycrystalline film. A calculation of this power has not been carried out, but it is clear that the power will be roughly equal to that already calculated, since the coupling constants, B^{ϵ} and B^{γ}, are nearly equal. Thus, it is reasonable to regard the dashed line in Fig. 7 as approximately $\frac{1}{2}$ the power from a polycrystalline film.

*Work supported in part by the NSF.

†Present address: Department of Electrical Engineering, University of Florida, Gainesville, Fl. 32601.

[1]T. K. Wagner and J. L. Stanford, Phys. Rev. B 1, 4488 (1970).
[2]L. W. Hart and J. L. Stanford, Phys. Rev. Lett. 27, 676 (1971).
[3]D. M. S. Bagguley and J. Liesegang, J. Appl. Phys. 37, 1220 (1966).
[4]F. C. Rossol and R. V. Jones, J. Appl. Phys. 37, 1227 (1966).
[5]B. R. Cooper, *Solid State Physics*, edited by F. Seitz and D. Turnbull (Academic, New York, 1968), Vol. 21, pp. 393–400.
[6]E. A. Turov and V. G. Shavrov, Fiz. Tverd. Tela 1, 217 (1965) [Sov. Phys.-Solid State 1, 1966 (1965)].
[7]B. R. Cooper, Phys. Rev. 169, 281 (1968).
[8]R. M. Nicklow, J. Appl. Phys. 42, 1672 (1971).
[9]D. T. Vigren and S. H. Liu, Phys. Rev. B 5, 2719 (1972).
[10]B. W. Southern and D. A. Goodings, Phys. Rev. B 7, 2028 (1973).
[11]H. Chow and F. Keffer, Phys. Rev. B 7, 2028 (1973).
[12]C. H. Anderson and E. S. Sabisky, *Physical Acoustics*, edited by W. P. Mason (Academic, New York, 1971), Vol. VIII, Chap. 1.
[13]R. M. White, M. Sparks, and I. Ortenburger, Phys. Rev. 139, A450 (1965).
[14]B. A. Auld, *Acoustic Fields and Waves in Solids* (Wiley, New York, 1973), Vol. 1, p. 130.
[15]E. Callen and H. B. Callen, Phys. Rev. 139, A455 (1967).
[16]M. T. Elliott, J. T. Wang, and H. A. Blackstead, Int. J. Magn. 6, 33 (1974).
[17]A. K. Ghatak and L. S. Kothari, *An Introduction to Lattice Dynamics* (Addison-Wesley, London, 1972), Chaps. 3–5.
[18]T. Holstein and H. Primakoff, Phys. Rev. 58, 1098 (1940).
[19]J. D. Jackson, *Classical Electrodynamics* (Wiley, New York, 1962), Chap. 8.
[20]J. J. Rhyne and A. E. Clark, J. Appl. Phys. 38, 1379 (1967).
[21]J. F. Elliott, S. Legvold, and F. H. Spedding, Phys. Rev. 94, 1143 (1954).
[22]M. T. Elliott, M. O'Donnell, and H. A. Blackstead, Phys. Rev. Lett. 32, 734 (1974).
[23]R. M. Bozorth and T. Wakiyama, J. Phys. Soc. Jpn. 18, 97 (1963).